2234

Nuclear Instruments and Methods in Physics Research B62 (1992) 463–468
North-Holland

Nuclear Instruments & Methods in Physics Research
Section B

The nature of keV and MeV ion damage in $Al_xGa_{1-x}As/GaAs$ and AlAs/GaAs heterostructures

A.G. Cullis [a], A. Polman [b], P.W. Smith [a], D.C. Jacobson [c], J.M. Poate [c] and C.R. Whitehouse [a]

[a] *DRA Electronics Division, Royal Signals and Radar Establishment, St Andrews Road, Malvern, Worcs WR14 3PS, UK*
[b] *FOM-Institute AMOLF, Kruislaan 407, 1098 SJ Amsterdam, The Netherlands*
[c] *AT & T Bell Laboratories, 600 Mountain Avenue, Murray Hill, New Jersey 07974, USA*

Received 19 July 1991

Bombardment damage produced by Si^+ ions in $Al_xGa_{1-x}As/GaAs$ layer structures has been studied using transmission electron microscopy, and ion channeling and backscattering spectrometry. The damage resistance of $Al_xGa_{1-x}As$ alloy layers increases with Al concentration. In particular, using complementary Si^+ ion doses yielding similar nuclear displacement densities at 150 keV and 2 MeV bombardment energies, it is demonstrated for the first time that the local concentration of implanted Si impurity is likely to be a significant factor in controlling lattice damage build up. It is also shown for the first time that, in a manner analogous to AlAs, the alloy layers can confer a significant protection from ion damage upon adjacent narrow zones of crystalline GaAs, which exhibit enhanced resistance to damage accumulation.

1. Introduction

Ion implantation of heterostructures followed by annealing can lead to intermixing of the constituent materials and this process has important applications in, for example, superlattice device fabrication [1,2]. However, the different crystalline materials which form the layers of such a structure can have different susceptibilities to lattice disorder production during the initial implantation, so that the overall disorder distribution may be inhomogeneous. Therefore, it is important to obtain a detailed understanding of implantation in heterostructures. A lot of work has focused on the $Al_xGa_{1-x}As/GaAs$ system. For binary AlAs/GaAs heterostructures, it has been demonstrated [3–5] that the AlAs is far more resistant to ion damage accumulation than the GaAs and, moreover, that the AlAs exerts a protective effect on adjacent narrow zones of GaAs crystal. For alloy $Al_xGa_{1-x}As/GaAs$ heterostructures, following observations on annealed material [6], it has been shown [7,8] that ion implantation disorder is also formed less readily in the alloy strata than in the GaAs, with an especially detailed study [9] of the production of disorder in alloy layers by heavy ion irradiation. Not only alloy compositions but also layer thicknesses have been found [10] to play a role in disorder production in superlattices.

In the present work, we examine Si^+ ion implantation damage in $Al_xGa_{1-x}As/GaAs$ layer structures in some detail. These studies focus on a direct comparison of the effects of keV and MeV ion bombardment and, by correlation with theoretical calculations, the likely influence of implanted Si impurity on lattice damage accumulation is deduced. We also highlight protection against ion damage accumulation, given by the alloy to adjacent layers of GaAs crystal.

2. Experimental details

Initial samples of the $Al_xGa_{1-x}As/GaAs$ heterostructures, with $x = 0.5, 0.7, 0.9$ and 1.0, were grown by molecular beam epitaxy. In each case, after deposition of a GaAs buffer layer on an (001) GaAs substrate, a single layer of the alloy (~ 100 nm thick) or AlAs (~ 90 nm thick) was grown, followed by a final ~ 70 nm capping layer of GaAs. Ion bombardment was carried out using $^{28}Si^+$ ions at an energy of either 150 keV or 2 MeV obtained from a 1.7 MV tandem accelerator and with samples tilted by ~ 7° from [001] and cooled to liquid nitrogen temperature (−196°C). General measurements of sample disorder were carried out by ion channeling and backscattering spectrometry using 2 MeV He^+ ions. Detailed structural studies were performed using a transmission electron microscope (TEM) operated at 400 kV and with samples thinned in cross-sectional configuration to electron transparency by low voltage Ar^+ ion milling, finishing (except for AlAs-containing samples) with I^+ ions to minimise residual milling damage [11].

3. Results

The as-grown heterostructure samples were examined in the TEM and found to be essentially defect-free, perfect single crystals. In order to determine the general behaviour of the alloy layers under ion bombardment and for comparison with our previous work [4] the samples were first implanted with 150 keV-Si^+ ions for doses in the range 10^{14}–10^{15} ions cm^{-2}. As shown in fig. 1(a), at an ion dose of 10^{14} cm^{-2} the $Al_{0.5}Ga_{0.5}As$ alloy layer exhibited point defect cluster disorder (giving dark dot contrast) after the bombardment but, nevertheless, was significantly less damaged than the adjacent GaAs which contained densely-packed point defect clusters interspersed with small amorphous regions. However, the $Al_{0.9}Ga_{0.1}As$ layer, see fig. 1(b), showed little lattice damage at this ion dose level. Indeed, this latter alloy layer protected the adjacent GaAs so that, as demonstrated in fig. 2, ~ 6 nm-wide zones of undamaged crystalline GaAs remained along the edges of the alloy, while other GaAs within the implantation envelope was heavily disordered or amorphized. This protection phenomenon is directly analogous to, although more limited than, that previously observed [4] to be produced by stoichiometric AlAs.

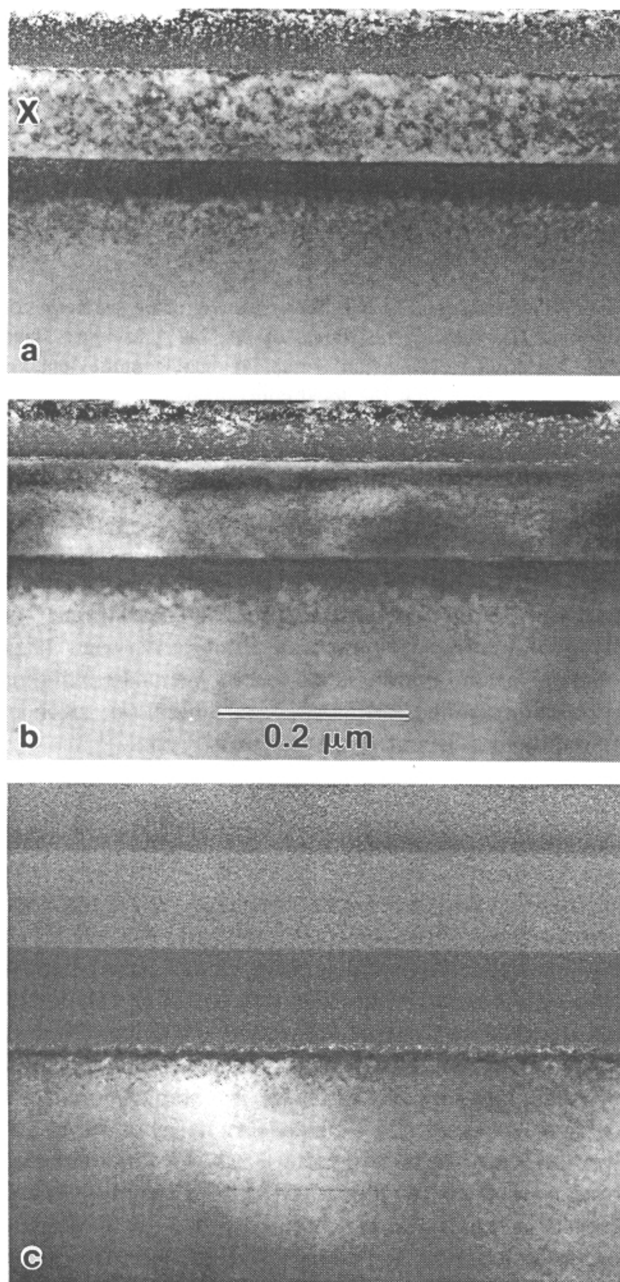

Fig. 1. Cross-sectional TEM images (g = $\bar{2}20$, dark field) of samples implanted with 150 keV Si^+ ions (a) 10^{14} ions cm^{-2} and $Al_{0.5}Ga_{0.5}As$ alloy layer (marked X) containing point defect clusters giving dark dot contrast, (b) 10^{14} ions cm^{-2} and $Al_{0.9}Ga_{0.1}As$ alloy layer exhibiting only dark/bright electron-optical contours and (c) 10^{15} ions cm^{-2} and $Al_{0.9}Ga_{0.1}As$ alloy layer which has been amorphized at this latter dose and shows uniform light contrast.

Fig. 2. Cross-sectional high resolution TEM image ([110] axial, bright field) of upper edge of crystalline $Al_{0.9}Ga_{0.1}As$ alloy layer after implantation of 1×10^{14} 150 keV Si^+ ions cm^{-2} showing protected crystalline GaAs zone (dark contrast between arrows) and overlying heavily damaged GaAs in the remainder of the cap.

When the incident ion dose was increased to 3×10^{14} Si^+ cm^{-2}, the disorder in the $Al_{0.5}Ga_{0.5}As$ alloy layer had saturated indicating the formation of an

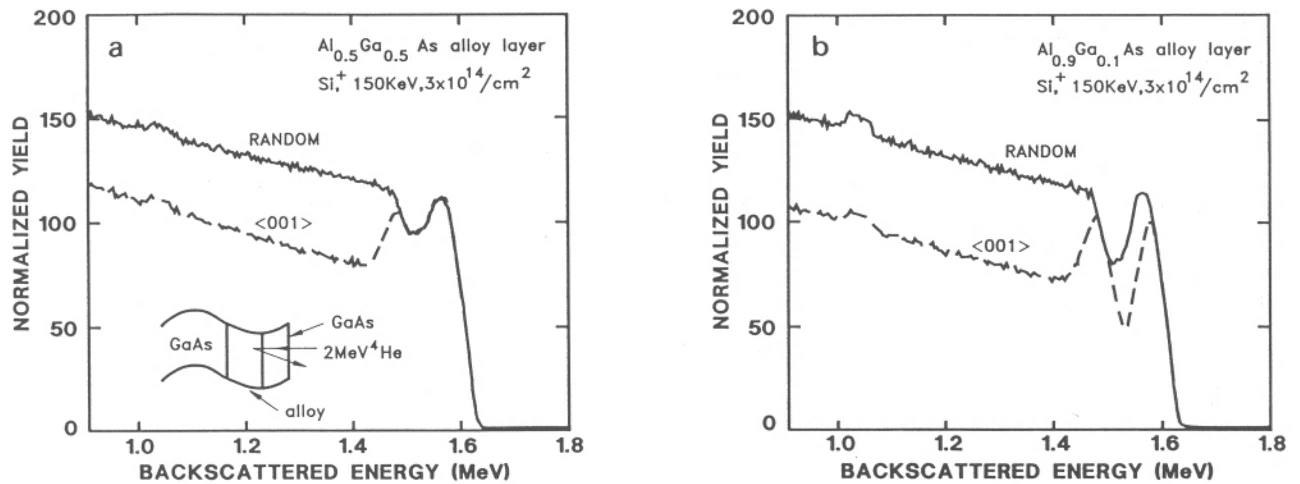

Fig. 3. Random and ⟨001⟩ channeled He^+ ion backscattering spectra from samples implanted with $3x10^{14}$ 150 keV Si^+ ions cm^{-2} (a) with $Al_{0.5}Ga_{0.5}As$ alloy layer and (b) with $Al_{0.9}Ga_{0.1}As$ alloy layer.

amorphous layer. This is clear from the He^+ ion backscattering spectrum in fig. 3(a) where the random and channeled yields are identical in the region exhibiting a depression corresponding to the presence of Al in the alloy layer. In contrast, the $Al_{0.9}Ga_{0.1}As$ layer still exhibited good crystallinity, since the backscattering spectrum of fig. 3(b) shows that the channeled ion yield was substantially below the 'random' level in the region corresponding to the alloy. However, when the higher Al-content alloy was subjected to ion bombardment at a dose of 10^{15} Si^+ ions cm^{-2}, it also was rendered completely amorphous as shown in fig. 1(c). Therefore, under these implantation conditions, it is clear that the $Al_{0.5}Ga_{0.5}As$ alloy is amorphized at an ion dose below 3×10^{14} cm^{-2}, whilst the $Al_{0.9}Ga_{0.1}As$ alloy resists amorphization up to an ion dose approaching 10^{15} cm^{-2}. Intermediate amorphisation behaviour was observed for the alloy sample with $x = 0.7$ and the ion doses required to form continuous amorphous layers in each of the alloys and GaAs are shown in fig. 4. The experimental curve is extrapolated to intersect the right-hand axis (corresponding to AlAs) at a point denoting a 150 keV Si^+ ion dose of just greater than 10^{16} cm^{-2}. However, this is an estimate, since amorphization of AlAs layers towards this dose level first takes place heterogeneously at layer boundaries [4] so that the bulk amorphization threshold is difficult to determine.

The disorder produced in the alloy layer samples by 2 MeV Si^+ ion implants has also been studied to give a direct comparison with the 150 keV ion case. After bombardment of the $Al_{0.5}Ga_{0.5}As$ layer sample with 1.5×10^{15} 2 MeV-Si^+ ions cm^{-2}, although the surrounding GaAs had been amorphized, the alloy retained good crystallinity but exhibited some point defect cluster disorder, as shown in fig. 5(a). However, an increase in the ion dose to 5×10^{15} 2 MeV-Si^+ ions cm^{-2} resulted in amorphization of the alloy (fig. 5(b)). In contrast, implantation of 1.5×10^{16} 2 MeV-Si^+ ions cm^{-2} into the $Al_{0.9}Ga_{0.1}As$ layer sample produced little detectable disorder of any type in the alloy (fig. 5(c)). The alloy sample with $x = 0.7$ again exhibited intermediate behaviour and the thresholds for formation of continuous amorphous layers by 2 MeV Si^+ ion bombardment in the different materials are shown along the upper curve in fig. 4. At this implantation energy, the data for the $x = 0.9$ alloy simply imply a lower bound for its amorphization threshold of $\sim$3-4 $\times 10^{16}$ ions cm^{-2}. Furthermore, layers of AlAs itself maintained essentially complete crystallinity up to a 2 MeV Si^+ ion dose of 5×10^{16} cm^{-2} (fig. 6) and careful

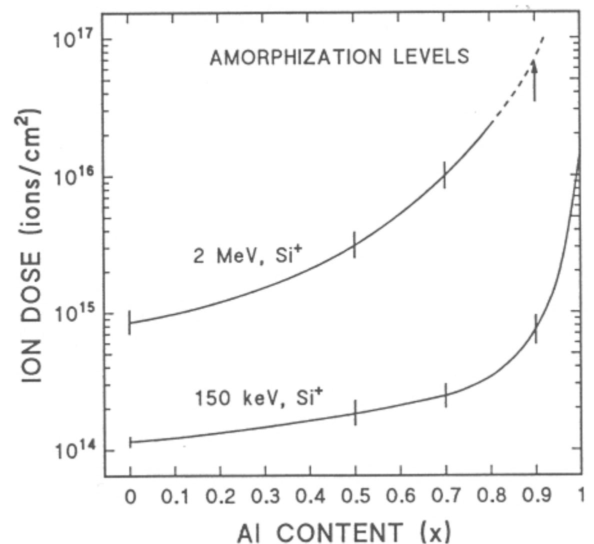

Fig. 4. The experimentally determined variation in amorphization thresholds for the $Al_xGa_{1-x}As$ alloys, together with GaAs and AlAs, at implanted Si^+ ion energies of 150 keV and 2 MeV.

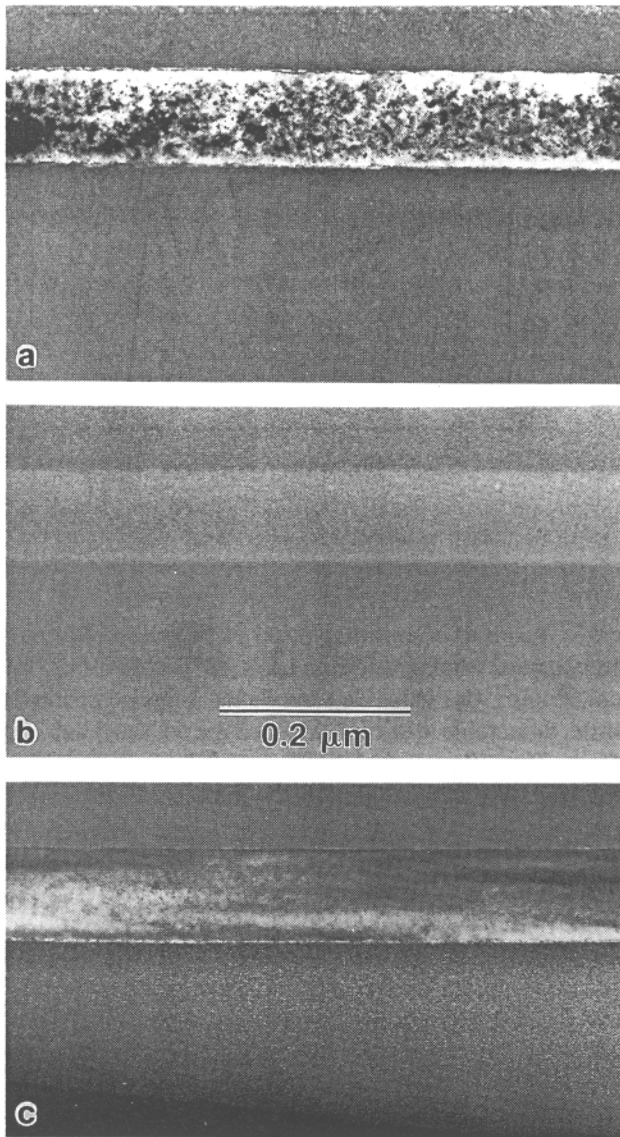

Fig. 5. Cross-sectional TEM images (g = $\bar{2}20$, dark field) of samples implanted with 2 MeV-Si^+ ions (a) 1.5x10^{15} ions cm^{-2} and $Al_{0.5}Ga_{0.5}As$ alloy layer containing point defect clusters giving dark dot contrast, (b) 5x10^{15} ions cm^{-2} and $Al_{0.5}Ga_{0.5}$ alloy layer which has been amorphized and shows uniform light contrast and (c) 1.5×10^{16} ions cm^{-2} and $Al_{0.9}Ga_{0.1}$ As alloy layer with few observable defects.

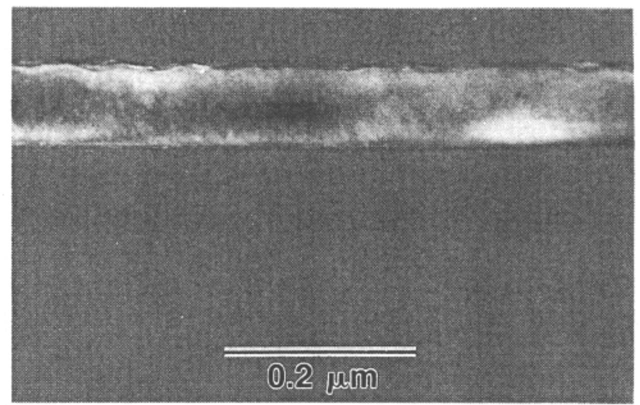

Fig. 6. Cross-sectional TEM image (g = $\bar{2}20$, dark field) of sample with AlAs buried layer after implantation with 5×10^{16} 2 MeV Si^+ ions cm^{-2}: the crystalline AlAs buried in amorphous GaAs exhibits dark/bright electron-optical contours, only.

measurements at high resolution showed that there was no diminution of AlAs layer width of the type seen previously [4] for $\geqslant 3\times10^{15}$ Si^+ ions cm^{-2} implanted at 150 keV. Thus, these observations indicate that the AlAs amorphization threshold is significantly greater than 10^{17} Si^+ ions cm^{-2} at the 2 MeV energy.

The densities of nuclear displacements produced by 150 keV and 2 MeV ions in $Al_xGa_{1-x}As$ alloys have been compared by simulation of the ion bombardment process with Monte Carlo computer calculations using the TRIM-89 program [12]. A displacement threshold energy of 15 eV/atom and a lattice binding energy of 1 eV/bond were assumed: displacements by recoiled target atoms were also taken into account. The predicted variation in nuclear displacement density with depth in a sample containing the $x = 0.9$ alloy layer is shown in fig. 7 and it is seen that, at any given dose level, 2 MeV ions produce $\sim$ 7–8 times fewer displacements in the alloy than 150 keV ions. This ratio remains constant to within $\sim$ 10% for alloy layers of all compositions. While the precise value of the ratio may be subject to some uncertainty due to approximations in the computer calculations employed, the significance of this basic result will be demonstrated in the next section.

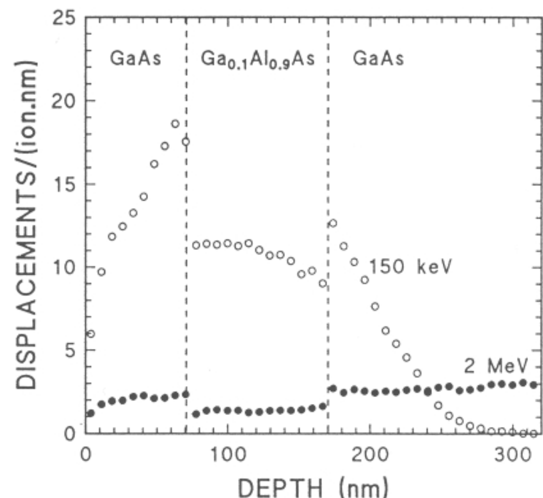

Fig. 7. Theoretically calculated variation of nuclear displacement density with depth for both 150 keV and 2 MeV $^{28}Si^+$ ion bombardment of a sample with a buried layer of $Al_{0.9}Ga_{0.1}As$ alloy.

4. Discussion

The present work has shown that, for Si^+ ion implantation in $Al_xGa_{1-x}As$ alloys at either 150 keV or 2 MeV energies, increasing Al concentration in the alloy also increases its ion damage resistance. While a very limited effect of this type is expected since the atomic mass of Al is lower than that of Ga (see fig. 7, where a GaAs-alloy displacement density differential of ~1.6 is evident) it is also clear from the experimental results of fig. 4 that the damage-resistance increases far beyond this level for the highest Al concentrations at both implantation energies, with AlAs showing extremely great resistance [4,5]. This phenomenon has previously been ascribed to the occurrence of in situ recrystallisation mediated by mobile point defects [3].

Fig. 4 shows a number of other features of particular importance. It is observed that the amorphization threshold of GaAs is ~7–8 times higher for ion bombardment at 2 MeV than at 150 keV. This can be considered to be reasonably in accord with the results of the Monte Carlo calculations, given the approximations employed in the latter. However, most importantly, the difference in amorphization thresholds at the two ion energies increases substantially with increasing Al concentration in the $Al_xGa_{1-x}As$ alloy, especially for x values greater than 0.5 and is, for example, a factor of ~40 for $x = 0.7$. Now, it is important to note that the amount of implanted Si present at the location of the alloy layer becomes quite large for implantation of high doses of ions at 150 keV, attaining ~1 at.% for a dose of 10^{16} Si^+ cm^{-2}. However, Monte Carlo simulations also confirm that the near surface Si present after a 2 MeV Si^+ ion dose of 10^{16} cm^{-2} only attains the parts-per-million level and, in general, the concentration is less than one part in 10^4 of that produced by 150 keV Si^+ ion bombardment at any given dose. While there are expected to be some characteristic differences in the nature of collision cascades produced at the two bombardment energies, based on the results of the simulations, such factors should be approximately constant across the alloy range. Thus, the observed large differential increase in damage-resistance, exhibited by the high-x alloys for 2 MeV Si^+ ion bombardment, is expected to be at least in part due to the low implanted impurity concentration. The very much higher Si concentrations incorporated during 150 keV implantations would be likely to impede in situ recrystallisation as conjectured previously [4], thus predisposing the III–V semiconductor lattice to premature breakdown and amorphization.

Furthermore, it has been demonstrated in the present work that, analogous to the case [4] of AlAs-containing heterostructures, although over a more limited dose range, the $Al_xGa_{1-x}As$ alloy is able to confer protection from the accumulation of ion-induced lattice disorder upon an immediately adjacent narrow zone of GaAs crystal. This phenomenon, once again, is likely to be associated with point defect diffusion and interaction between the two materials, the thickness of the GaAs protected zones being, perhaps, related to the defect diffusion length.

It is finally interesting to note that the Al-concentration-dependent disorder resistance of the alloy itself, combined with the ion-energy-dependence of the damage and the presence of protection zones in the GaAs would render the prediction of superlattice disorder thresholds quite complex, as is observed experimentally [10].

5. Conclusions

In the present work we have shown that there are characteristic differences in the amorphization thresholds of $Al_xGa_{1-x}As$ alloys and AlAs for Si^+ ion bombardment at keV and MeV energies. By correlating observations with the results of computer simulations, it is deduced that the differences in the concentration of implanted Si are likely to play a key role in determining the variation in relative disorder-formation and amorphization thresholds at the two energies. Furthermore, the general trend of enhanced damage resistance for the alloys with higher Al concentrations may be associated with mobile point defect behaviour. The latter is also likely to be responsible for the damage protection now observed to be conferred upon GaAs crystal neighbouring alloy layers in the heterostructures.

Acknowledgements

The authors would like to thank M.T. Emeny (RSRE) for the MBE growth of the samples used in this work and Dr. D.J. Eaglesham (AT&T Bell Labs) for helpful discussions. Copyright C Controller, HMSO, London, 1991.

References

[1] P.G. Deppe and N. Holonyak, Jr., J. Appl. Phys. 64 (1988) R93.

[2] M. Kawabe, N. Matsuara, N. Shimizu, F. Hasegawa and Y. Nannichi, Jpn. J. Appl. Phys. 23 (1984) L623.

[3] A.G. Cullis, N.G. Chew, C.R. Whitehouse, D.C. Jacobson, J.M. Poate and S.J. Pearton, Appl. Phys. Lett. 55 (1989) 1211.

[4] A.G. Cullis, P.W. Smith, D.C. Jacobson and J.M. Poate, J. Appl. Phys. 69 (1991) 1279.

[5] D.J. Eaglesham, J.M. Poate, D.C. Jacobson, M. Cerullo, L.N. Pfeiffer and K. West, Appl. Phys. Lett. 58 (1991) 523.

[6] J. Ralston, G.W. Wicks, L.F. Eastman, B.C. DeCooman and C.B. Carter, J. Appl. Phys. 59 (1986) 120.

[7] K. Matsui, T. Takamori, T. Fukunaga, T. Narusawa and H. Nakashima, Jpn. J. Appl. Phys. 26 (1987) 482.

[8] S.-Tong Lee, G. Braunstein, P. Fellinger, K.B. Kahen and G. Rajeswaren, Appl. Phys. Lett. 53 (1988) 2531.

[9] I. Jenčič, M.W. Bench, I.M. Robertson and M.A. Kirk, J. Appl. Phys. 69 (1991) 1287.

[10] E.A. Dobisz, H. Dietrich, A.W. McCormick and J.P. Harbison, Mater. Res. Soc. Symp. Proc. 147 (1989) 285.

[11] N.G. Chew and A.G. Cullis, Ultramicroscopy 23 (1987) 175.

[12] J.P. Biersack and L.J. Haggmark, Nucl. Instr. and Meth. 174 (1980) 257.